

Diastereoselective Intramolecular C–H bond Activation by Optically Active Tris(pyrazolyl)hydroborate Complexes of Rhodium

Michael C. Keyes, Victor G. Young, Jr., and William B. Tolman*

Department of Chemistry, University of Minnesota, 207 Pleasant Street SE, Minneapolis, Minnesota 55455

Received February 9, 1996[⊗]

Results are reported of photolyses of rhodium dicarbonyl complexes of C_3 -symmetric Tp^{Menth} and $\text{Tp}^{\text{Mementh}}$ ligands that illustrate the capability of these scorpionates to exhibit a high degree of regio- and stereocontrol in reactions involving intramolecular attack of ligand substituent C–H bonds. The starting material $\text{Tp}^{\text{Menth}}\text{Rh}(\text{CO})_2$ was found to contain an η^2 - Tp^{Menth} ligand in the solid state by X-ray crystallography but was shown to be an interconverting mixture of η^2 and η^3 forms in toluene solution by IR and NMR spectroscopy. A mechanism for the fluxionality based on one previously suggested for achiral systems was supported by line shape analysis of VT-NMR data. Irradiation of $\text{Tp}^{\text{Menth}}\text{Rh}(\text{CO})_2$ under a N_2 purge in a variety of solvents resulted in the generation of an 85:15 mixture of diastereomeric alkyl hydrides resulting from intramolecular cyclometalation reactions involving the methyl substituents on the ligand isopropyl group. Analysis of two-dimensional NMR data (DQ-COSY, NOESY, HMQC, TOCSY spectra) allowed assignment of all ^1H and ^{13}C resonances arising from the functionalized pyrazolyl group and identification of the R - C_J , R -Rh absolute configurations of these new stereocenters in the major product. Various evidence, including spin-saturation transfer NMR and kinetics data, is reported that suggests (i) the minor isomer differs only in the configuration at C_J and (ii) that the major and minor isomers thermally equilibrate via a mechanism involving rate-limiting alkyl–hydride reductive elimination and subsequent oxidative addition to either methyl group of the same pyrazolyl unit without inversion of configuration at the metal. The net result is cyclometalation with complete enantiocontrol at the rhodium center.

The development of processes in which carbon–hydrogen bonds are cleaved selectively by transition metal complexes is an important research objective, particularly in view of their significance in biological systems and potential applications in organic synthesis and industrial catalysis.¹ Despite extensive advances in delineating the fundamentals of C–H bond activations involving oxidative additions to coordinatively unsaturated rhodium or iridium complexes,^{2–5} research oriented toward developing enantio- or diastereoselective variants is in its infancy.⁶ We recently synthesized a series of optically active tris(pyrazolyl)hydroborate (Tp^{RR})^{7–9} ligands and their complexes¹⁰ as part of an effort to understand the role of higher-order rotational symmetry in enantioselective processes and to develop

new stereoselective reactions. The known photochemical efficiency of C–H activations by rhodium complexes of achiral Tp^{RR} ligands⁴ led us to consider that analogs containing our chiral pyrazoles might carry out such reactions stereoselectively. We report (i) studies of the solution and solid state structures of rhodium dicarbonyl complexes of C_3 -symmetric Tp^{Menth} and $\text{Tp}^{\text{Mementh}}$ ligands (Chart 1) and (ii) results of photolyses of these compounds that illustrate the capability of the chiral scorpionates to exhibit a high degree of regio- and

* Author to whom correspondence should be addressed. E-mail: tolman@chem.umn.edu. FAX: 612-624-7029.

[⊗] Abstract published in *Advance ACS Abstracts*, September 1, 1996.
(1) (a) Arndtsen, B. A.; Bergman, R. G.; Mobley, T. A.; Peterson, T. H. *Acc. Chem. Res.* **1995**, *28*, 154–162. (b) Crabtree, R. H. In *The Chemistry of Alkanes and Cycloalkanes*; Patai, S., Rappaport, Z., Eds.; Wiley Interscience: New York, 1992; pp 653–679. (c) Crabtree, R. H. *Chem. Rev.* **1985**, *85*, 245–269.

(2) (a) Bengali, A. A.; Schultz, R. H.; Moore, C. B.; Bergman, R. G. *J. Am. Chem. Soc.* **1994**, *116*, 9585–9589. (b) Mobley, T. A.; Schade, C.; Bergman, R. G. *J. Am. Chem. Soc.* **1995**, *117*, 7822–7823. (c) Partridge, M. G.; McCamley, A.; Perytz, R. N. *J. Chem. Soc., Dalton Trans.* **1994**, 3519–3526. (d) Mobley, T. A.; Schade, C.; Bergman, R. G. *J. Am. Chem. Soc.* **1995**, *117*, 7822–7823. (e) Bromberg, S. E.; Lian, T.; Bergman, R. G.; Harris, C. B. *J. Am. Chem. Soc.* **1996**, *118*, 2069–2072. (f) Lian, T.; Bromberg, S. E.; Yang, H.; Proulx, G.; Bergman, R. G.; Harris, C. B. *J. Am. Chem. Soc.* **1996**, *118*, 3769–3770.

(3) (a) Wang, C.; Ziller, J. W.; Flood, T. C. *J. Am. Chem. Soc.* **1995**, *117*, 1647–1648. (b) Wang, L.; Wang, C.; Bau, R.; Flood, T. C. *Organometallics* **1996**, *15*, 491–498.

(4) (a) Ghosh, C. K.; Graham, W. A. G. *J. Am. Chem. Soc.* **1987**, *109*, 4726–4727. (b) Ghosh, C. K.; Hoyano, J. K.; Krentz, R.; Graham, W. A. G. *J. Am. Chem. Soc.* **1989**, *111*, 5480–5481. (c) Krentz, R. Ph.D. Thesis, University of Alberta, 1989. (d) Jones, W. D.; Hessel, E. T. *Inorg. Chem.* **1991**, *30*, 778–783. (e) Jones, W. D.; Hessel, E. T. *J. Am. Chem. Soc.* **1992**, *114*, 6087–6095. (f) Jones, W. D.; Hessel, E. T. *J. Am. Chem. Soc.* **1993**, *115*, 554–562. (g) Perez, P. J.; Poveda, M. L.; Carmona, E. *Angew. Chem., Int. Ed. Engl.* **1995**, *34*, 231–233. (h) Purwoko, A. A.; Lees, A. J. *Inorg. Chem.* **1995**, *34*, 424–425. (i) Purwoko, A. A.; Drolet, D. P.; Lees, A. J. *Organomet. Chem.* **1995**, *504*, 107–117. (j) Purwoko, A. A.; Lees, A. J. *Inorg. Chem.* **1996**, *35*, 675–682.

(5) Crabtree, R. H.; Holt, E. M.; Lavin, M.; Morehouse, S. M. *Inorg. Chem.* **1985**, *24*, 1986–1992.

(6) Ma, Y.; Bergman, R. G. *Organometallics* **1994**, *13*, 2548–2550. Correction: *Organometallics* **1994**, *13*, 4648.

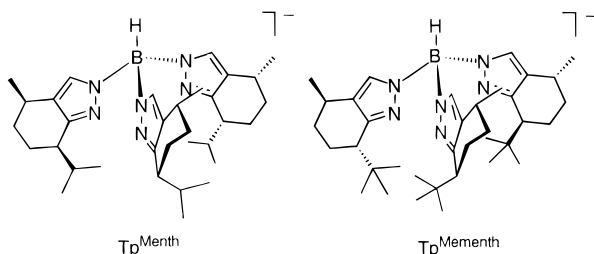
(7) The abbreviation system is that reported in ref 8b, where Tp^{RR} = hydrotris(3-R-5-R'-pyrazol-1-yl)borate.

(8) Reviews on Tp chemistry: (a) Trofimenko, S. *Prog. Inorg. Chem.* **1986**, *34*, 115–210. (b) Trofimenko, S. *Chem. Rev.* **1993**, *93*, 943–980. (c) Kitajima, N.; Tolman, W. B. *Prog. Inorg. Chem.* **1995**, *43*, 419–531. (d) Parkin, G. *Adv. Inorg. Chem.* **1995**, *42*, 291–393.

(9) LeCloux, D. D.; Tokar, C. J.; Osawa, M.; Houser, R. P.; Keyes, M. C.; Tolman, W. B. *Organometallics* **1994**, *13*, 2855–2866.

(10) LeCloux, D. D.; Keyes, M. C.; Osawa, M.; Reynolds, V.; Tolman, W. B. *Inorg. Chem.* **1994**, *33*, 6361–6368.

Chart 1



stereocontrol in reactions involving intramolecular attack of ligand substituent C–H bonds.

Results and Discussion

Synthesis and Structures of $\text{Tp}^*\text{Rh}(\text{CO})_2$.

The starting materials $\text{Tp}^*\text{Rh}(\text{CO})_2$ ($\text{Tp}^* = \text{Tp}^{\text{Menth}}$ or $\text{Tp}^{\text{Mementh}}$) were prepared by metathesis of the respective TiTp^* with $[\text{Rh}(\text{CO})_2\text{Cl}]_2$ in CH_2Cl_2 as described previously¹⁰ but using an improved workup procedure that allowed isolation of the Tp^{Menth} complex as yellow crystals in high yield (83% vs 21% reported earlier). We have not been able to isolate $\text{Tp}^{\text{Mementh}}\text{Rh}(\text{CO})_2$ in analytically pure form so far, but solids exhibiting diagnostic IR and NMR spectroscopic features with only minor amounts of impurities detectable by these methods were prepared and used in preliminary photochemical experiments (vide infra). An X-ray crystal structure of $\text{Tp}^{\text{Menth}}\text{Rh}(\text{CO})_2$ (Figure 1; selected distances and angles listed in Table 1) revealed η^2 coordination of Tp^{Menth} to a square planar rhodium dicarbonyl fragment, a binding mode seen previously in several other like complexes of sterically hindered $\text{Tp}^{\text{RR'}}$ ligands.¹¹ Two pyrazolyl groups are coordinated to rhodium by short Rh–N bonds (average 2.09 Å) with the third N-donor oriented away from the axial coordination position and weakly hydrogen-bonded to a disordered CH_2Cl_2 solvent molecule [not shown; $\text{N}(31)\cdots\text{C}(1\text{A}) = 3.4796(8)$ Å; $\text{N}(31)\cdots\text{C}(1\text{B}) = 3.4551(4)$ Å]. This boat configuration (Figure 1B) also was found in crystalline $\text{Tp}^{\text{Ph}}\text{Rh}(\text{CO})_2$, but it differs from an alternate boat geometry observed for $\eta^2\text{-Tp}^{\text{CF}_3\text{Me}}\text{Rh}(\text{CO})_2$ and $\eta^2\text{-Tp}^{\text{a}}\text{Rh}(\text{CO})_2$, in which the third uncoordinated N-donor points toward the axial position ($\text{Rh}-\text{N} = 2.6\text{--}2.7$ Å).¹¹ As discussed below, in solution $\text{Tp}^{\text{Menth}}\text{Rh}(\text{CO})_2$ interconverts between these two boat geometries.

The IR spectra of solid $\text{Tp}^{\text{Menth}}\text{Rh}(\text{CO})_2$ and $\text{Tp}^{\text{Mementh}}\text{Rh}(\text{CO})_2$ (KBr pellets) contain two sharp bands at 2077, 2006 cm^{-1} and 2076, 2009 cm^{-1} , respectively, consistent with η^2 -coordination as indicated by X-ray crystallography for the Tp^{Menth} complex (Figure 2A). Two additional shoulders at 2056 and 1978 cm^{-1} are also apparent in the spectrum of $\text{Tp}^{\text{Menth}}\text{Rh}(\text{CO})_2$ that are diagnostic of $\eta^3\text{-Tp}^{\text{RR'}}$ coordination in an 18-electron 5-coordinate complex. This spectrum was obtained as a KBr pellet of crushed crystals from the batch used for the X-ray structure determination, so either the conversion of the η^2 form to the η^3 isomer is facile in the solid state or the two forms are present in the batch

(11) (a) $\eta^2\text{-Tp}^{\text{CF}_3\text{Me}}\text{Rh}(\text{CO})_2$ and $\eta^2\text{-Tp}^{\text{Ph}}\text{Rh}(\text{CO})_2$: Krentz, R. Model Compounds in Carbon-Hydrogen Catalysis. Ph.D. Thesis, University of Alberta, Edmonton, Canada, 1989. (b) $\eta^2\text{-Tp}^{\text{a}}\text{Rh}(\text{CO})_2$ [$\text{Tp}^{\text{a}} = \text{hydrotris}(2\text{H-benz}[g]-4,5\text{-dihydroindazol-2-yl})\text{borate}$]: Rheingold, A. L.; Ostrander, R. L.; Haggerty, B. S.; Trofimenko, S. *Inorg. Chem.* **1994**, *33*, 3666–3676.

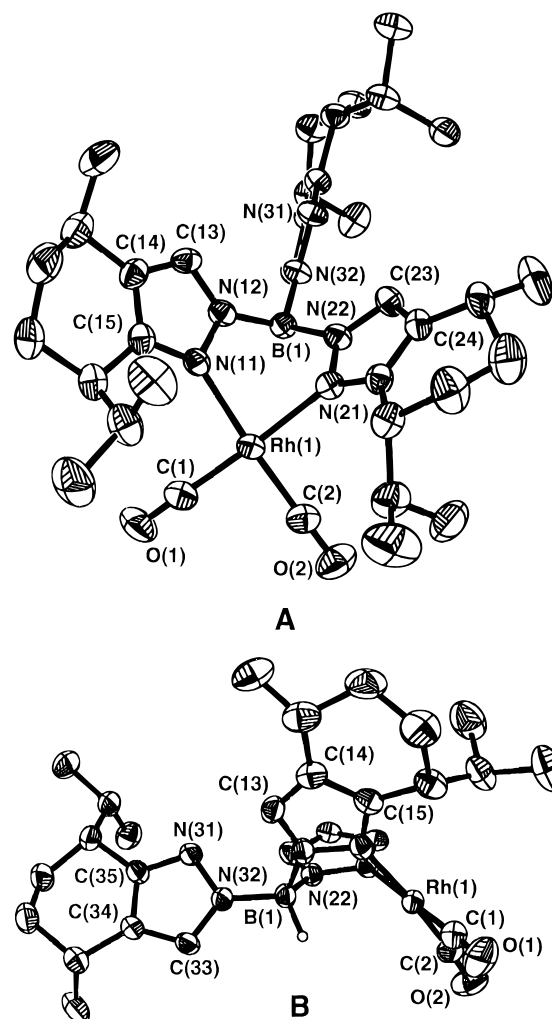


Figure 1. Representations of the X-ray crystal structure of $\text{Tp}^{\text{Menth}}\text{Rh}(\text{CO})_2$ showing non-hydrogen atoms as 50% thermal ellipsoids and selected atom labels (CH_2Cl_2 solvate omitted for clarity). In (B) the pyrazole substituent atoms of the rear pyrazole unit have been omitted for clarity.

Table 1. Selected Bond Lengths (Å) and Bond Angles (deg) for $\text{Tp}^{\text{Menth}}\text{Rh}(\text{CO})_2 \cdot \text{CH}_2\text{Cl}_2$

Rh1–C1	1.853(3)	Rh1–C2	1.854(3)
Rh1–N11	2.082(2)	Rh1–N21	2.105(2)
C1–O1	1.142(4)	B1–N12	1.553(4)
B1–N32	1.510(4)	N11–C15	1.357(4)
B1–N22	1.560(4)	N12–C13	1.348(4)
N11–N12	1.366(3)	N21–C25	1.354(4)
N21–N22	1.372(4)	N22–C23	1.347(4)
N31–N32	1.384(3)	N31–C35	1.333(3)
		N32–C33	1.366(4)
C1–Rh1–C2	89.41(14)	C1–Rh1–N11	174.3(2)
C2–Rh1–N11	92.48(12)	C1–Rh1–N21	93.54(12)
C2–Rh1–N21	176.2(2)	N11–Rh1–N21	84.36(9)
O1–C1–Rh1	176.5(4)	O2–C2–Rh1	179.5(4)
N32–B1–N12	110.6(2)	N32–B1–N22	111.4(2)
N12–B1–N22	105.4(2)	C15–N11–N12	107.5(2)
C15–N11–Rh1	138.0(2)	N12–N11–Rh1	114.3(2)
C13–N12–N11	108.6(2)	C13–N12–B1	133.0(2)
N11–N12–B1	118.4(2)	N12–C13–C14	109.4(3)
N11–C15–C16	123.6(3)	N11–C15–C14	109.4(3)
C25–N21–Rh1	139.5(2)	C25–N21–N22	107.1(2)
C23–N22–N21	109.1(2)	N22–N21–Rh1	113.4(2)
N21–N22–B1	117.9(2)	C23–N22–B1	131.8(2)
N21–C25–C26	126.3(3)	N22–C23–C24	109.1(3)
C35–N31–N32	105.3(2)	N21–C25–C24	109.0(3)

as separate crystals, only one of which was chosen for the X-ray crystallographic analysis. The η^2 coordination

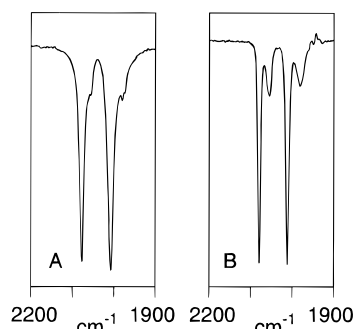


Figure 2. Carbonyl stretching region of the IR spectra of recrystallized $\text{Tp}^{\text{Menth}}\text{Rh}(\text{CO})_2$ as a KBr pellet (A) and as a toluene solution (B).

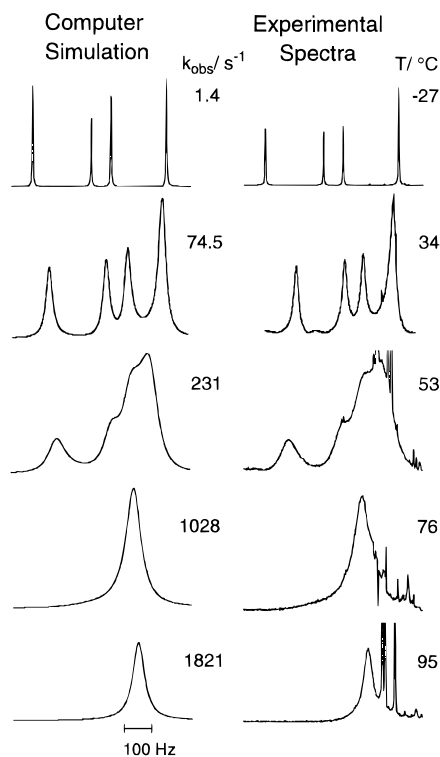
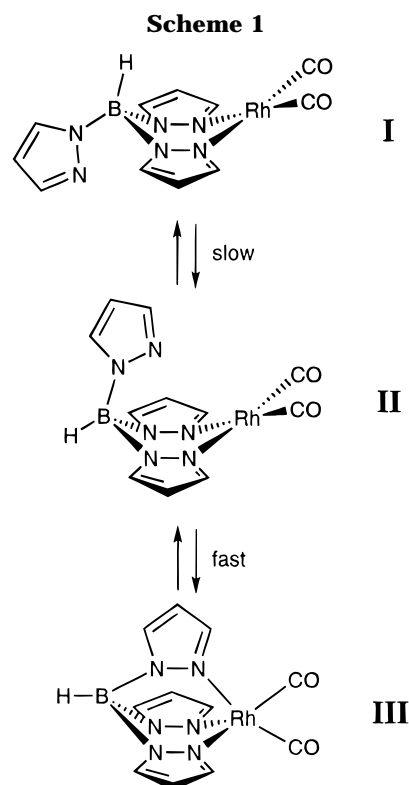


Figure 3. 500 MHz variable-temperature experimental and simulated NMR spectra of the pyrazole proton region (6.9–8 ppm) of $\text{Tp}^{\text{Menth}}\text{Rh}(\text{CO})_2$ in toluene- d_8 . Extra peaks in the higher field region of the experimental spectra at higher temperatures are indicative of partial sample decomposition.

mode is retained in solution for $\text{Tp}^{\text{Menth}}\text{Rh}(\text{CO})_2$, as shown by its solution IR spectrum [ν_{CO} (pentane) = 2080, 2012 cm^{-1}] and the presence of a 1:1:1 ratio of pyrazolyl ring hydrogen peaks (7–8 ppm region) in its ^1H NMR spectrum in toluene- d_8 arising from the lack of a mirror plane in the optically pure chiral molecule. In contrast, the solution structure of $\text{Tp}^{\text{Menth}}\text{Rh}(\text{CO})_2$ is complicated by fluxionality. Two sets of bands are present in a 80:20 ratio in the IR spectrum of the complex in toluene (Figure 2B), one pair at 2080 and 2011 cm^{-1} corresponding to the square planar η^2 - Tp^{Menth} structure and another at 2055 and 1981 cm^{-1} attributable to η^3 - Tp^{Menth} coordination. Equilibration between the η^2 and η^3 forms is apparent in variable-temperature ^1H NMR spectra of a solution of the complex in toluene- d_8 (Figure 3). In the pyrazolyl ring hydrogen region at low temperature three peaks in a 1:1:1 ratio plus a fourth singlet are apparent (ratio of set of three peaks



to the fourth is 56:44). All four peaks coalesce upon heating and revert to their original form upon cooling.

Our interpretation of this behavior follows from an analysis recently reported by Venanzi and co-workers for some achiral $\text{Tp}^{\text{RR}}\text{Rh}(\text{CO})_2$ systems.¹² We suggest that the set of three peaks in 1:1:1 ratio corresponds to the η^2 structure **I** (Scheme 1) adopted by $\text{Tp}^{\text{Menth}}\text{Rh}(\text{CO})_2$ in the crystal analyzed by X-ray methods. The fourth single peak we assign to two isomers that interconvert in a fast fluxional process, one being the alternative boat form **II** of the crystallographically determined η^2 structure and the other being the η^3 isomer **III**. This rapid interconversion involving alternating pyrazolyl association and dissociation randomizes the pyrazolyl ring environments, resulting in a single peak in the NMR spectrum. Although **I** and **II** are sufficiently structurally similar to render them indistinguishable in the solution IR spectrum, **III** is observable and can be quantitated. By using the combined NMR and IR peak integration data (vide supra), we calculate that **I–III** coexist in toluene at room temperature in a ratio of 56:24:20. According to the pathway shown in Scheme 1, the mechanism responsible for the coalescence behavior observed by variable-temperature NMR spectroscopy involves a slow interconversion of the two boat forms **I** and **II** of the η^2 isomer. Because one of them, **II**, rapidly interconverts with the η^3 form in a process that randomizes the pyrazolyl ring environments, the net process is equivalent to equilibration between four nuclear configurations: three η^2 structures **I**, with each pyrazolyl ring uncoordinated in turn, and one symmetrical structure **III** (equilibrating with **II** in a process too fast to be observed). Line-shape analysis using this model¹³ yielded calculated spectra in good agreement with the experimental VT NMR data (Figure 3) and afforded

(12) Bucher, U. E.; Currao, A.; Nesper, R.; Rügger, H.; Venanzi, L. M.; Younger, E. *Inorg. Chem.* **1995**, *34*, 66–74.

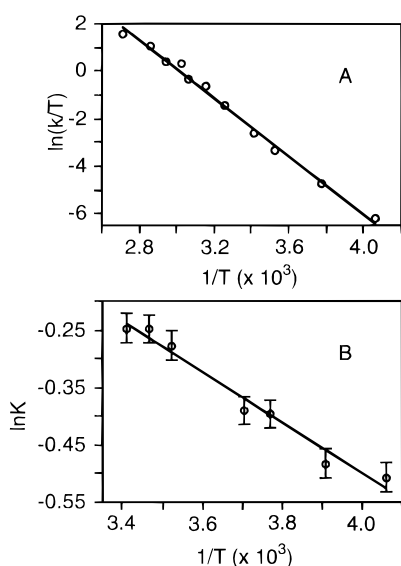


Figure 4. Eyring (A) and van't Hoff plots (B) for the equilibration of configuration **I** of $\text{Tp}^{\text{Menth}}\text{Rh}(\text{CO})_2$ with configuration **II/III** derived from variable-temperature NMR data: $\Delta H^\ddagger = 12 \pm 0.5 \text{ kcal mol}^{-1}$; $\Delta S^\ddagger = -11 \pm 2 \text{ eu}$; $\Delta H = 1.0 \pm 0.5 \text{ kcal mol}^{-1}$; $\Delta S^\circ = 2.5 \pm 1 \text{ eu}$.

activation parameters via an Eyring analysis (Figure 4A): $\Delta H^\ddagger = 12 \pm 0.5 \text{ kcal/mol}$; $\Delta S^\ddagger = -11 \pm 2 \text{ eu}$. Thermodynamic parameters for the equilibrium **I** \rightleftharpoons **II/III** were calculated from a van't Hoff plot of integration data (Figure 4B): $\Delta H = 1.0 \pm 0.5 \text{ kcal/mol}$; $\Delta S^\circ = 2.5 \pm 1 \text{ eu}$. Solution fluxional behavior analogous to that which we have been able to analyze in detail for $\text{Tp}^{\text{Menth}}\text{Rh}(\text{CO})_2$ has been postulated for other $\text{Tp}^{\text{RR}}\text{Rh}(\text{CO})_2$ complexes^{4,8c,11} and thus may be viewed as a general characteristic of this class of compounds. Its importance has been underscored by Purwoko and Lees,^{4h-j} who have demonstrated that the η^2 and η^3 forms exhibit divergent photochemical C–H bond activation reactivity.

C–H Bond Activation Chemistry. Photolysis of yellow solutions of $\text{Tp}^{\text{Menth}}\text{Rh}(\text{CO})_2$ with broad band UV–visible radiation (projector lamp) in a range of solvents (C_6D_6 , pentane, toluene, THF, Et_2O) caused rapid decolorization and, when performed with an N_2 purge, clean generation of an 85:15 mixture of two rhodium hydride species indicated by doublets at -14.39 and -14.55 ppm with $J_{\text{Rh-H}} = 25.0$ and 24.3 Hz , respectively, in the ^1H NMR spectrum (Figure 5). A $\nu_{\text{Rh-H}}$ at 2077 cm^{-1} was also identified in the IR spectrum. The products were isolated as an air-stable solid; attempts to functionalize the hydrides by halogens or halogenated solvents failed (decomposition to intractable mixtures). The product composition was not influenced by the nature of the solvent, clearly indicating that intermolecular C–H activation is disfavored. Instead, the combined analytical, mass spectral, and IR and NMR spectroscopic data are consistent with an intramolecular reaction to generate diastereomeric alkyl hydrides derived from activation of methyl C–H bonds

of a pyrazolyl isopropyl substituent of Tp^{Menth} (Scheme 2).

Faced with a lack of crystals suitable for X-ray crystallographic analysis, we used two-dimensional NMR methods (DQ-COSY, NOESY, HMQC,¹⁴ TOCSY¹⁵) to determine the structure and absolute stereochemistry of the major product. The NMR assignments are listed in Table 2, and complete 2D NMR data are provided as Supporting Information (Figures S1–S4). In brief, the assignments were obtained by first identifying the hydrogen and carbon atoms associated with each respective pyrazolyl unit using ^1H – ^1H (DQ-COSY, TOCSY) and ^1H – ^{13}C (HMQC) correlation data. Specific ^1H NMR assignments were obtained primarily through analysis of the COSY data, as exemplified for the cyclometalated ring system in Figure 6. Stereochemical assignments were then derived from the NOESY spectrum data, the correlations shown in Figure 7 being key determinants of the absolute configurations of stereocenters C_j and Rh. Thus, a correlation between H_f and methyl group H_k supports the indicated *R* configuration for C_j , while a correlation between methyl group H_k and the Rh–H also reveals an *R* configuration for the Rh atom.

Complete assignment of the absolute configuration of the minor diastereomer was more problematic because of significant spectral overlap with the major product. The available evidence indicates that the stereochemistry of the minor product is inverted at C_j but retains the same configuration at Rh. In other words, the other isopropyl methyl group is activated with identical stereochemistry at the metal compared to the major isomer. In support of this hypothesis, the ^1H NMR spectrum of the solution resulting from irradiation of $\text{Tp}^{\text{Menth}}\text{Rh}(\text{CO})_2$ contained only one Rh–H doublet at -14.77 ppm ($J_{\text{Rh-H}} = 25.1 \text{ Hz}$). Although the ^1H NMR spectrum is consistent with an intramolecular C–H bond activation analogous to that observed for Tp^{Menth} , in this instance decomposition and spectral overlaps precluded full assignment of the product. Nonetheless, because the quaternary *tert*-butyl carbon in Tp^{Menth} cannot become a new stereogenic center in the intramolecular reaction, the observation of a single Rh–H signal indicates the formation of a single diastereomer and implies complete (within NMR detection limits) stereochemical control at the Rh center for this reaction and, by extrapolation, for the Tp^{Menth} case as well.

Also consistent with the notion that the major and minor products of the photolysis of $\text{Tp}^{\text{Menth}}\text{Rh}(\text{CO})_2$ arise from attack at either of the two isopropyl substituent methyl groups with the same stereochemistry at the metal was our finding that the two products rapidly equilibrate and that the 85:15 ratio is thermodynamically controlled (Scheme 2). Irradiation of $\text{Tp}^{\text{Menth}}\text{Rh}(\text{CO})_2$ at $-78 \text{ }^\circ\text{C}$ yielded a 40:60 mixture that transformed in a gradual thermal process to the final 85:15 ratio of isomeric alkyl hydrides. The final ratio did not vary appreciably between -13 and $22 \text{ }^\circ\text{C}$. Rate constants (k_{obs}) for the conversion were obtained from the slopes of linear ($R > 0.994$) first-order plots of the integrated areas of the hydride resonances in ^1H NMR spectra monitored over time at selected temperatures

(13) Stephenson, D. S.; Binsch, G. Converted and modified by LeMaster, C. B.; LeMaster, C. L.; True, N. S. *DNMR5: Iterative Nuclear Magnetic Resonance Program for Unsaturated Exchange-Broadened Bandshapes, QCPE Program No. QCMP059*; IBM-PC edition; Quantum Chemistry Program Exchange: Indiana University, Bloomington, IN, 1988.

(14) Summers, M. F.; Marzilli, L. G.; Bax, A. *J. Am. Chem. Soc.* **1986**, *108*, 4285–4294.

(15) Bax, A.; Davis, D. G. *J. Magn. Reson.* **1985**, *65*, 355–360.

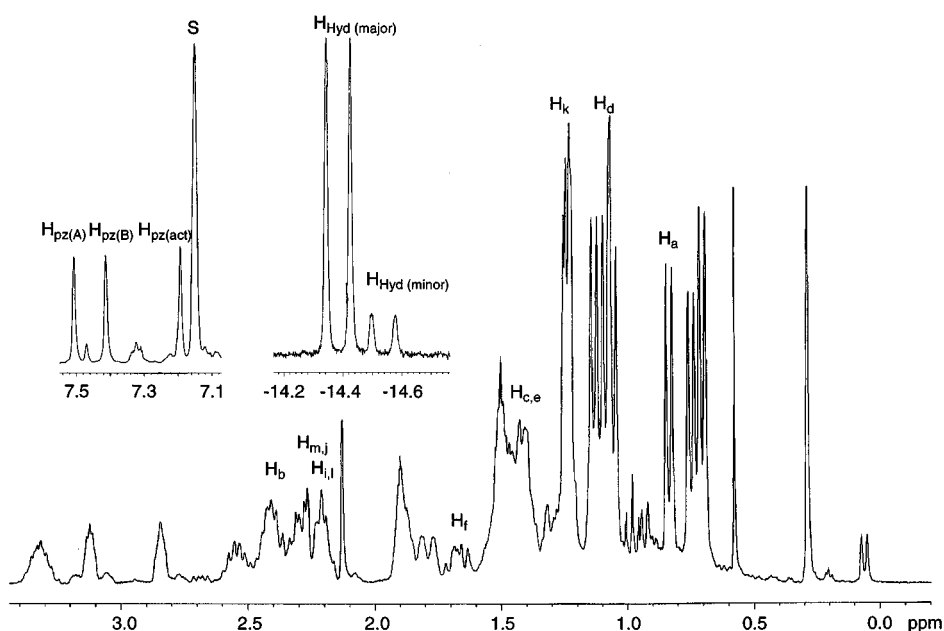
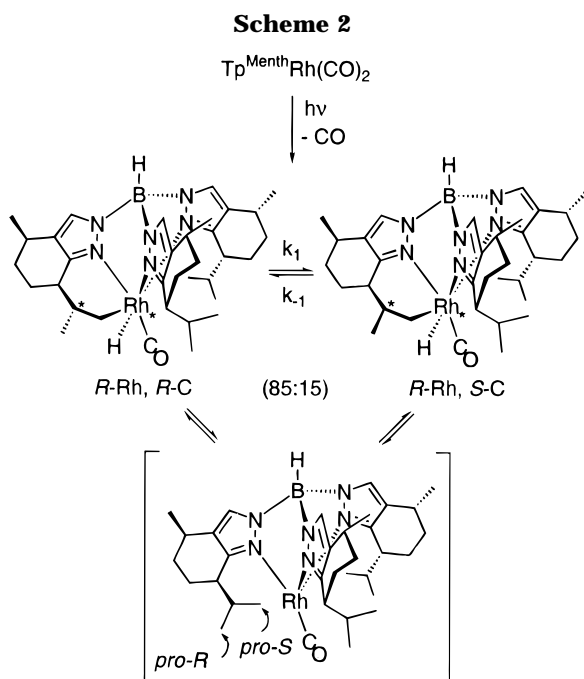


Figure 5. 300 MHz ^1H NMR spectrum of irradiated $\text{Tp}^{\text{Menth}}\text{Rh}(\text{CO})_2$ in C_6D_6 with assignments for the cyclometalated pyrazole unit and the hydrides (see Figure 7 and Table 2 for the structural assignments). The vertical scales of the insets differ from each other and from the main spectrum.



in the range -13 to $+10$ $^{\circ}\text{C}$. A representative first-order plot is presented in the Supporting Information (Figure S6). Because of the reversible nature of the interconversion of the isomers the observed first-order rate constants (k_{obs}) are actually the sum of the forward and reverse rate constants, $k_1 + k_{-1}$.¹⁶ Since $K_{\text{eq}} = k_1/k_{-1}$ is known ($=15/85 = 0.176$), we were able to calculate values of k_1 and k_{-1} and then subject them to an Eyring analysis (Figure 8) to obtain activation parameters for the individual reaction steps. The values for the forward and reverse steps are essentially the same within experimental error; for k_1 , $\Delta H^{\ddagger} = 20 \pm 2$ kcal mol $^{-1}$, $\Delta S^{\ddagger} = -2 \pm 5$ eu, and $\Delta G^{\ddagger}_{298} = 21$ kcal mol $^{-1}$.

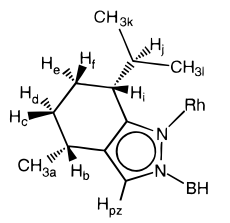
We propose that this equilibration involves a rate-limiting alkyl-hydride reductive elimination to a coordinatively unsaturated intermediate, perhaps via an alkane complex, that oxidatively adds to a different methyl group (Scheme 2). This path inverts the C_J configuration without affecting the absolute configuration at the metal. The activation parameters we have measured fall within the range of values previously reported for reductive eliminations of alkanes from rhodium alkyl hydride complexes supported by Tp or Cp ligands ($\Delta G^{\ddagger}_{298} = 20\text{--}24$ kcal mol $^{-1}$),^{4f,17} lending support to our hypothesis of reductive elimination as the slow step in the isomerization reaction. Consistent with the intermediacy of a coordinatively unsaturated intermediate (or one weakly bound to a C-H bond) that can be trapped, treatment of the photolysis product mixture with CO (1 atm) caused complete reversion to the $\text{Tp}^{\text{Menth}}\text{Rh}(\text{CO})_2$ starting material. Further support for the reductive elimination/oxidative addition mechanism shown in Scheme 2 was obtained from two-dimensional spin saturation exchange NMR experiments at 50 $^{\circ}\text{C}$ (shown in Supporting Information Figure S5). Exchange cross-peaks (also seen as negative peaks in the NOESY spectrum) were observed between the unactivated isopropyl methyl group (H_k) of the cyclometalated pyrazole and the metal hydride, indicating that the equilibration between the major and minor photoproducts involves the reversible cyclometalation of the two methyls on the *same* isopropyl group (labeled *pro-R* and *pro-S* in Scheme 2).^{2b}

Conclusion

In sum, we have delineated the solution- and solid-state structural features and fluxional energetics of the optically pure $\text{Tp}^{\text{Menth}}\text{Rh}(\text{CO})_2$ complex through combined X-ray crystallographic and variable-temperature NMR and IR spectroscopic studies. Both η^2 - and η^3 -

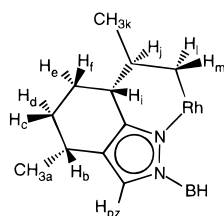
(16) Espenson, J. H. *Chemical Kinetics and Reaction Mechanisms*; McGraw Hill: New York, 1981; pp 42–44.

(17) Jones, W. D.; Feher, F. J. *J. Am. Chem. Soc.* **1984**, *106*, 1650–1663.

Table 2. NMR Peak Assignments of Irradiated $\text{Tp}^{\text{Menth}}\text{Rh}(\text{CO})_2$


Pyrazole A			
^1H NMR		^{13}C NMR	
δ (ppm)	proton	δ (ppm)	carbon ^a
0.75 (d) ^b	CH_{3k}	18.7-19.0	C_k
1.1 (d) ^b	CH_{3a}	21-22	C_a, C_1
1.2 (d) ^b	CH_{3l}	22-23	C_{ef}
1.3 (m)	H_d	26-27	C_b
1.5 (m)	H_f, H_c	29.5-30.5	$\text{C}_{cd}, \text{C}_j$
1.9 (m)	H_e	37.9	C_i
2.4 (m)	H_b	132.6	C_{pz}
3.1 (m)	H_i		
3.3 (m)	H_j		
7.5 (s)	H_{pz}		

Pyrazole B			
^1H NMR		^{13}C NMR	
δ (ppm)	proton	δ (ppm)	carbon ^a
0.70 (d) ^b	CH_{3k}	18.7-19.0	C_k
1.05 (d) ^b	CH_{3a}	21-22	C_a, C_1
1.12 (d) ^b	CH_{3l}	22-23	C_{ef}
1.25 (m)	H_c	26-27	C_b
1.41 (m)	H_d	29.5-30.5	C_{cd}
1.47 (m)	H_f	32.4	C_i
1.80 (m)	H_e	37.5	C_j
2.3 (m)	H_b	131.5	C_{pz}
2.54 (m)	H_i		
2.81 (m)	H_j		
7.41 (s)	H_{pz}		



Cyclometallated Pyrazole			
^1H NMR		^{13}C NMR	
δ (ppm)	proton	δ (ppm)	carbon ^a
-14.39 (d) ^c	$\text{H}_{\text{Hydride}}$	16.7	C_{Im}^d
0.83 (d) ^b	CH_{3a}	21-22	C_k, C_a
1.13 (m)	H_d	25-27	$\text{C}_{ef}, \text{C}_i, \text{C}_b$
1.25 (d) ^b	CH_{3k}	29.5-30.5	C_{cd}
1.4 (m)	H_c, H_e	42.8	C_j
1.68 (m)	H_f	129.8	C_{pz}
2.2 (m)	H_i, H_l		
2.3 (m)	H_m, H_j		
2.4 (m)	H_b		
7.19 (m)	H_{pz}		

^aAssignments from HMQC and DEPT spectra. Carbons are labeled by the letter(s) of the attached protons. ^b $J = 7.0$ Hz. ^c $J = 25$ Hz. ^d $J = 20$ Hz.

Tp^{Menth} coordination modes have been identified and activation parameters for the interconversion of two η^2 boat geometries have been obtained. In addition, the optically active C_3 -symmetric Tp^{Menth} and Tp^{Menth} ligands have been shown to control the stereoselectivity

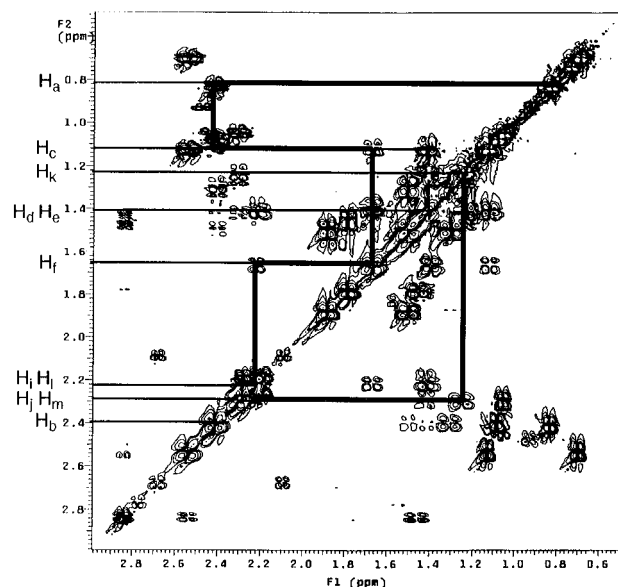


Figure 6. A region of the 500 MHz DQ-COSY spectrum of irradiated $\text{Tp}^{\text{Menth}}\text{Rh}(\text{CO})_2$ with assignments for the cyclometallated pyrazole unit (see Figure 7 and Table 2 for the structural assignments). The bold line denotes a "walk" through the spin system of the cyclometallated pyrazole.

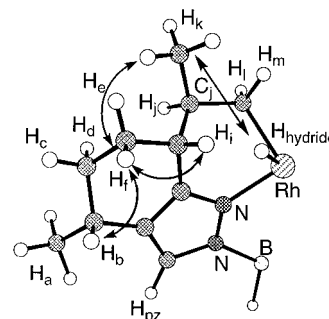


Figure 7. Structural assignments and key NOESY correlations of the hydrogens of the cyclometallated pyrazole unit in the major product formed upon photolysis of $\text{Tp}^{\text{Menth}}\text{Rh}(\text{CO})_2$.

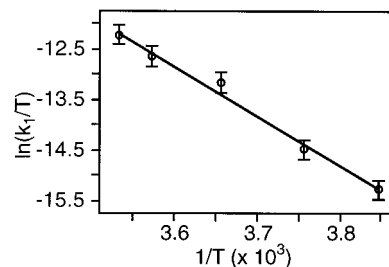


Figure 8. Eyring plot for the equilibration of the major and minor products of the irradiation of $\text{Tp}^{\text{Menth}}\text{Rh}(\text{CO})_2$: $\Delta H^\ddagger = 20 \pm 2$ kcal mol⁻¹; $\Delta S^\ddagger = -2 \pm 5$ eu.

of C–H bond activation by their coordinated rhodium centers, as evinced by high overall diastereoselectivity and complete enantiocontrol at the metal in their cyclometalation reactions. Kinetic parameters and spin-saturation exchange data are consistent with an intramolecular thermal process that interconverts the cyclometallated diastereomers via a mechanism involving sequential reductive elimination and oxidative addition reactions. Although cyclometallated analogs resulting from irradiation of other complexes of achiral, sterically hindered $\text{Tp}^{\text{RR'}}$ ligands (e.g., Tp^{iPr} or Tp^{Ph_2}) are capable of undergoing intermolecular C–H bond

activation reactions when thermodynamically driven,^{4c} the species derived from the Tp^{Menth} and Tp^{Menth} complexes are unreactive toward pentane, benzene, or cyclopropane solvents. The lack of reactivity of our chiral hydrido-alkyls toward exogenous reagents apparently derives from the extreme steric bulk of the ligands, which prevent addition of all but the smallest substrates (CO). Attaining enantioselective intermolecular C–H bond activation may therefore necessitate the development of less hindered optically active polypyrazolyl ligands and complexes.

Experimental Section

General Procedures. All air-sensitive reactions were performed either in a Vacuum Atmospheres glovebox under an N_2 atmosphere or by using standard Schlenk and vacuum-line techniques. The synthesis of $\text{TiTp}^{\text{Menth}}$ and $\text{TiTp}^{\text{Menth}}$, as well as general procedures used for synthesis and characterization, have been described.⁹ NMR experiments were carried out on a Varian VXR-500 or VXR-300 spectrometer using standard parameters.

$\text{Tp}^{\text{Menth}}\text{Rh}(\text{CO})_2$. In a glovebox, $\text{TiTp}^{\text{Menth}}$ (101 mg, 0.13 mmol) and $[\text{Rh}(\text{CO})_2\text{Cl}]_2$ (26 mg, 0.13 mmol) were stirred in CH_2Cl_2 (3 mL) for 10 min. The solvent was evaporated, the yellow residue was dissolved in pentane (2 mL), and the solution was filtered through a Celite pad. The Celite pad was washed with pentane (1 mL), and the combined pentane solutions were evaporated to dryness. The resulting yellow solid was recrystallized from $\text{CH}_2\text{Cl}_2/\text{CH}_3\text{CN}$ to yield large yellow crystals (78 mg, 83% yield). Characterization data were identical to those obtained for material synthesized according to the previously published method,¹⁰ except for the IR of the crystalline material which is primarily $\eta^2\text{-Tp}^{\text{Menth}}\text{Rh}(\text{CO})_2$. IR (KBr): 2955, 2476 (B–H), 2077 (CO), 2006 (CO), 1554, 1452, 1369, 1157 cm^{-1} .

Analysis of the Fluxionality of $\text{Tp}^{\text{Menth}}\text{Rh}(\text{CO})_2$ in Solution. $\text{Tp}^{\text{Menth}}\text{Rh}(\text{CO})_2$ (15 mg) was dissolved in toluene- d_6 , and the tube was sealed under an N_2 atmosphere. NMR spectra were taken at 13 temperatures ranging from -30 to $+100$ °C. Each temperature was determined using either a methanol or ethylene glycol standard. Line shape and integration analysis of the pyrazole region (6.5–8 ppm) was carried out at each temperature using DNMR5.¹³ The system was modeled as an equilibration between four nuclear configurations as described in the text with $T_2 = 0.1355$. Since the peak positions and the relative population of each state varied with temperature, the variation of these values was measured at low temperature (below 25 °C in the case of the peak positions, below 45 °C for the populations) and extrapolated to higher temperatures.

Irradiation of $\text{Tp}^{\text{Menth}}\text{Rh}(\text{CO})_2$. This procedure is a modification of that published by Krentz for achiral analogs.^{4c} $\text{Tp}^{\text{Menth}}\text{Rh}(\text{CO})_2$ (50 mg, 0.071 mmol) was dissolved in pentane (50 mL) in a Pyrex Schlenk flask fitted with a rubber septum. Dry nitrogen was slowly bubbled through the solution, and the flask was placed in a water/ice bath. Irradiation (82 V, 410 W overhead projector lamp attached to a Variac set at 45) resulted in complete bleaching of the yellow solution in 30 min. Removal of the solvent in vacuo yielded an off white powder which consisted of two diastereomeric products (85:15 ratio at room temperature) by ^1H NMR spectroscopy. Recrystallization from $\text{CH}_2\text{Cl}_2/\text{CH}_3\text{CN}$ yielded an analytically pure white powder (33 mg, 0.05 mmol, 70% yield). IR (KBr): 2952, 2277 (B–H), 2073, 2024 (CO), 1554, 1453, 1414, 1394, 1373, 1367, 1313, 1140, 1104 cm^{-1} . ^{13}C NMR (125 MHz, C_6D_6): δ 192.7 (d, $J = 66$ Hz, Rh–CO), 153.0, 152.9, 15.06, 132.6, 131.4, 129.8, 122.3, 121.6, 121.5, 42.8, 37.9, 37.5, 37.3, 32.4, 30.5, 30.1, 29.3, 27.0, 26.7, 26.1, 25.9, 23.2, 22.3, 22.2, 21.8, 21.6, 21.3, 21.2, 19.1, 18.8, 16.7 (d, $J = 20$ Hz) ppm (32 out of 33 expected peaks). FABMS (MNBA matrix) m/z : 675

($[\text{M} + \text{H}]^+$). Anal. Calcd for $\text{BC}_{34}\text{H}_{52}\text{N}_6\text{ORh}$: C, 60.54; H, 7.77; N, 12.46. Found: C, 60.79; H, 7.86; N, 12.16.

Alternatively, $\text{Tp}^{\text{Menth}}\text{Rh}(\text{CO})_2$ (3 mg, 0.00427 mmol) was dissolved in 0.75 mL of deuterated solvent (benzene- d_6 , toluene- d_8 , pentane- d_{12} , or tetrahydrofuran- d_8). This solution was then flame sealed under vacuum in an NMR tube, and the tube was irradiated with the overhead lamp described above or in a Rayonet photochemical reactor with 366 nm bulbs. Low-temperature irradiations were carried out by cooling the sealed tube to -70 °C in a MeOH/dry ice bath during irradiation with the overhead lamp. Yield: 100% (by NMR for 0 °C irradiations).

Irradiation of $\text{Tp}^{\text{Menth}}\text{Rh}(\text{CO})_2$. A CH_2Cl_2 (1 mL) solution of $\text{TiTp}^{\text{Menth}}$ (50 mg, 0.0063 mmol) was mixed with a solution of $[\text{CIRh}(\text{CO})_2]_2$ (12.9 mg, 0.0034 mmol) in CH_2Cl_2 (0.5 mL) for 15 min. The brown/black precipitate was removed by filtration, and solvent was removed *in vacuo* from the bright yellow filtrate to yield a yellow/brown solid, identified as $\text{Tp}^{\text{Menth}}\text{Rh}(\text{CO})_2$ from IR and NMR spectroscopy. IR (KBr): 2964, 2476 (B–H), 2076 (CO), 2009 (CO), 1130 cm^{-1} . IR (in pentane): 2060 (CO), 2012 (CO) cm^{-1} . ^1H NMR (C_6D_6 , 300 MHz): δ 7.86 (s, 1H), 7.47 (s, 1H), 7.27 (s, 1H), 2.78–2.85 (m, 3H), 2.35–2.55 (m, 5H), 1.5–1.9 (m, 9H), 0.5–1.3 (m, 10H), 1.07 (s, 9H), 0.95 (s, 9H), 0.84 (s, 9H) ppm. The solid was dissolved in 20 mL of pentane, the solution was cooled to 0 °C, and it was irradiated for 30 min with the overhead projector lamp while purging with N_2 . The sample turned dark brown during irradiation. The solvent was removed *in vacuo*, and the brown residue was identified as the alkyl-hydride complex through analysis of IR and NMR spectral data (no starting material indicated). IR (KBr): 2077 (Rh–H), 1974 (CO) cm^{-1} . ^1H NMR (C_6D_6 , 300 MHz): δ 7.58 (s, 1H), 7.31 (s, 2H), 3.25 (m, 1H), 3.0 (m, 1H), 2.55 (m, 2H), 2.2–2.5 (m, 3H), 1.5–2.0 (m, 9H), 1.15–1.4 (m, 4H) 1.02 (s, 9H), 0.98 (d, $J = 7$ Hz, 3H), 0.91 (d, $J = 7$ Hz, 3H), 0.90 (d, $J = 7$ Hz, 3H) 0.86 (s, 9H), 0.28 (s, 3H), -0.17 (s, 3H), -14.77 (d, $J_{\text{Rh}} = 25.4$ Hz, 1H).

CO Reversion Experiment. A sample of $\text{Tp}^{\text{Menth}}\text{Rh}(\text{CO})_2$ (20 mg) in pentane (20 mL) was irradiated at 0 °C with a N_2 purge. CO gas was then purged through the sample for 30 min, and the sample was stirred under a CO atmosphere at room temperature for 24 h. The pentane was then removed to afford a yellow powder. Clean reversion to $\text{Tp}^{\text{Menth}}\text{Rh}(\text{CO})_2$ was evident from IR, UV-vis, and ^1H NMR spectroscopic analysis.

Kinetics of the Isomerization of the Major and Minor Isomers of Irradiated $\text{Tp}^{\text{Menth}}\text{Rh}(\text{CO})_2$. A solution of $\text{Tp}^{\text{Menth}}\text{Rh}(\text{CO})_2$ (3 mg) in 0.6 mL of pentane- d_{12} and toluene- d_8 (1:1 v/v) was placed under static vacuum in an NMR tube. The tube was cooled to -78 °C (dry ice/acetone in a silvered dewar) and was irradiated at this temperature for 30 min with the projection lamp. The tube was re-evacuated, sealed, and placed in the precooled (-20 °C) NMR spectrometer probe. Spectra were taken periodically at -20 °C or other selected temperatures until the equilibration to the final 85:15 ratio of products was complete. The observed rate constants were determined from the slopes of first-order plots of the relative intensities of the hydride peaks.

X-ray Crystallography. A yellow block-shaped crystal of $\text{Tp}^{\text{Menth}}\text{Rh}(\text{CO})_2 \cdot \text{CH}_2\text{Cl}_2$ was attached to a glass fiber and mounted on the Siemens SMART system for data collection at 173(2) K. Cell constants were determined as described previously.¹⁸ A semiempirical absorption correction afforded minimum and maximum transmission factors of 0.4572 and 0.5078, respectively. See Table 3 for additional crystal and refinement information. The space group $P2_12_12_1$ was determined on the basis of systematic absences and intensity statistics, and a successful direct methods solution was calculated which provided most non-hydrogen atoms from the

(18) Halfen, J. A.; Mahapatra, S.; Wilkinson, E. C.; Gengenbach, A. J.; Young, V. G., Jr.; Que, L., Jr.; Tolman, W. B. *J. Am. Chem. Soc.* **1996**, *118*, 763–776.

Table 3. Crystallographic Data for $\text{Tp}^{\text{Menth}}\text{Rh}(\text{CO})_2\cdot\text{CH}_2\text{Cl}_2$

formula	$\text{C}_{36}\text{H}_{53}\text{BCl}_2\text{N}_2\text{O}_2\text{Rh}$
fw	786.46
space group	$P2_12_12_1$ (No. 19)
a (Å)	12.7818(6)
b (Å)	16.2502(8)
c (Å)	19.1846(9)
V (Å ³)	3984.8(3)
Z	4
ρ_{calcd} (Mg/m ³)	1.311
abs coeff (mm ⁻¹)	0.601
temp (°C)	-100(2)
radiation, λ (Å)	Mo K α , 0.710 73
$2\theta_{\text{max}}$ (deg)	48.22
reflens collcd	17 025
indepdt reflcns ^a	6234
no. of variable params	461
final $R1^a$ [$I > 2\sigma(I)$]	0.0282
$wR2^b$ [$I > 2\sigma(I)$]	0.0295
largest diff peak and hole (e Å ⁻³)	0.630, -0.377

^a $R1 = \sum ||F_o| - |F_c|| / \sum |F_o|$. $wR2 = [\sum [w(F_o^2 - F_c^2)^2] / \sum [w(F_o^2)^2]]^{1/2}$, where $w = 1 / [q\sigma^2(F_o^2) + (aP)^2 + bP]$.

E-map. Several full-matrix least-squares/difference Fourier cycles were performed which located the remainder of the non-hydrogen atoms, all of which were refined with anisotropic displacement parameters. The final structure was found with one solvent molecule of CH_2Cl_2 disordered over two sites (refined to a 79:21 ratio). Drawings of the structure appear in Figure 1, and selected bond lengths and angles are

contained in Table 1. Full details of the structure determination, including tables of bond lengths and angles, atomic positional parameters, and final thermal parameters for non-hydrogen atoms, are given in the Supporting Information. All calculations were performed using SGI INDY R4400-SC or Pentium computers with the SHELXTL-Plus V5.0 program suite.¹⁹

Acknowledgment. This work was supported by the National Science Foundation (Grant CHE-9207152 to W.B.T., a National Young Investigator Award to W.B.T., and Grant CHE-9413114 for partial funding for the Siemens SMART system) and the Camille and Henry Dreyfus and Alfred P. Sloan Foundations (fellowships to W.B.T.). We thank Dr. Mark Rosen for his assistance with the two-dimensional NMR experiments.

Supporting Information Available: Full details of the X-ray structure of $\text{Tp}^{\text{Menth}}\text{Rh}(\text{CO})_2\cdot\text{CH}_2\text{Cl}_2$ including text describing X-ray procedures, ORTEP diagrams, and tables of atomic coordinates and *U* values, bond lengths, bond angles, and anisotropic thermal parameters and two-dimensional NMR spectra of irradiated $\text{Tp}^{\text{Menth}}\text{Rh}(\text{CO})_2$ (19 pages). Ordering information is given on any current masthead page.

OM960093M

(19) SHELXTL-Plus V5.0, Siemens Industrial Automation, Inc., Madison, WI.